AAC
Journals.ASM.org

Synchrotron X-Ray Fluorescence Microscopy of Gallium in Bladder Tissue following Gallium Maltolate Administration during Urinary Tract Infection

Katherine R. Ball,[a] Francesca Sampieri,[a] Manuel Chirino,[b] Don L. Hamilton,[a] Robert I. R. Blyth,[c] Tsun-Kong Sham,[d] Patricia M. Dowling,[a] Julie Thompson[c]

Department of Veterinary Biomedical Sciences, Western College of Veterinary Medicine, University of Saskatchewan, Saskatoon, Saskatchewan, Canada[a]; Department of Veterinary Microbiology, Western College of Veterinary Medicine, University of Saskatchewan, Saskatoon, Saskatchewan, Canada[b]; Canadian Light Source, Inc., University of Saskatchewan, Saskatoon, Saskatchewan, Canada[c]; Department of Chemistry, University of Western Ontario, Chemistry Building, London, Ontario, Canada[d]

A mouse model of cystitis caused by uropathogenic *Escherichia coli* was used to study the distribution of gallium in bladder tissue following oral administration of gallium maltolate during urinary tract infection. The median concentration of gallium in homogenized bladder tissue from infected mice was 1.93 μg/g after daily administration of gallium maltolate for 5 days. Synchrotron X-ray fluorescence imaging and X-ray absorption spectroscopy of bladder sections confirmed that gallium arrived at the transitional epithelium, a potential site of uropathogenic *E. coli* infection. Gallium and iron were similarly but not identically distributed in the tissues, suggesting that at least some distribution mechanisms are not common between the two elements. The results of this study indicate that gallium maltolate may be a suitable candidate for further development as a novel antimicrobial therapy for urinary tract infections caused by uropathogenic *E. coli*.

Urinary tract infections (UTIs) are common in humans and dogs, and most of these infections are caused by uropathogenic strains of *Escherichia coli* (UPEC) (1, 2). In addition to patient discomfort and economic burdens from treatment costs and lost work time, failure to cure these infections can lead to serious complications, including pyelonephritis and septicemia (3). Antimicrobial resistance in UPEC complicates therapy and is of concern for both canine and human patients because these pathogens may be zoonotic (4–6). An increasing prevalence of antimicrobial resistance among UPEC from human and canine patients has created a need for a new approach to treatment (2, 7–9).

Uropathogenic strains of *E. coli* are distinguished by their ability to invade and persist in the urinary tract (10). By invading the transitional epithelial cells, UPEC are able to evade many host defenses and can persist in the urinary tract despite the presence of bactericidal concentrations of antimicrobial drugs in urine (11, 12). The virulence of UPEC is associated with genes coding for siderophores and siderophore receptors, suggesting that siderophore iron uptake pathways are essential for UPEC survival in the urinary tract (10, 13). Compounds which arrive at the transitional epithelium and interfere with bacterial iron metabolism may therefore be suitable alternatives to traditional antimicrobial therapy.

The element gallium, as gallium(III), is similar in size and behavior to iron(III) (14). Unlike iron(III), gallium(III) is not known to undergo reduction under physiological conditions (14). Gallium binds readily to transferrin, and its transport in mammalian tissues is thought to depend on transferrin receptor pathways (15). The similarities between gallium and iron also affect bacterial systems. *In vitro*, gallium binds to *E. coli* siderophores and exerts antimicrobial activity against Gram-negative and intracellular pathogens by disrupting iron metabolism (16–18). The salts gallium citrate and gallium nitrate are used in human medicine for medical imaging and treating hypercalcemia of malignancy, respectively, but they must be administered intravenously due to negligible oral bioavailability. Gallium maltolate, a complex of gallium(III) with three maltol groups, is of particular interest as a potential UTI therapy as it can be administered orally (19).

While gallium distribution has been described in a limited number of tissues, its distribution in the urinary bladder is unknown (15, 20). Confirmation of gallium distribution to the transitional epithelium following oral administration of gallium maltolate will support further investigation of gallium maltolate as a new antimicrobial therapy for UTIs caused by UPEC.

Metal detection by analytical methods such as inductively coupled plasma mass spectrometry require tissue homogenization, possibly with centrifugal separation or fine dissection to achieve a sample suitable for introducing into the instrument. Hard X-ray microprobe analysis is a synchrotron-based analytical technique which includes synchrotron X-ray fluorescence (XRF) imaging and X-ray absorption spectroscopy (XAS). Synchrotrons are electron accelerators which generate intense, focused X-rays that can be used to probe the electron structure of atoms within a variety of sample types, yielding valuable information about the distribution and chemical characteristics of elements within the sample. Elements of interest in intact samples can be localized on a micron scale using XRF imaging, and XAS can be used to determine the species of the elements of interest in regions of interest in the sample (21, 22). Hard X-ray microprobe analysis has been used to evaluate the distribution of elements in a variety of biological samples, including cardiac muscle, macrophages, and neurons (21, 23,

Received 27 March 2013 **Returned for modification** 4 May 2013
Accepted 14 July 2013
Published ahead of print 22 July 2013
Address correspondence to Katherine R. Ball, katherine.ball@usask.ca.

doi:10.1128/AAC.00616-13

24). As tissue homogenization is not required for analysis, these methods are well suited for investigating the distribution of metal-based drugs within tissues.

The objectives of this study were to use a well-characterized mouse model of UPEC cystitis, XRF imaging, and XAS to confirm the arrival of gallium in the bladder mucosa after oral administration of gallium maltolate (25). The relationship of gallium and iron distribution was also investigated to gain insight into potential mechanisms for gallium distribution in the bladder.

MATERIALS AND METHODS

Mice. All procedures involving mice were approved by the University of Saskatchewan Committee for Animal Care (protocol 20080060). Six 8- to 10-week-old female C56BL/6 mice were anesthetized with isoflurane and infected transurethrally with 10^8 CFU of a canine clinical uropathogenic *Escherichia coli* isolate (M2B, isolated at the Western College of Veterinary Medicine Bacteriology Laboratory) in a volume of 50 μl as previously described (25). Treatments were started 48 h after infection. Three mice received gallium maltolate (provided by Lawrence Bernstein) in distilled water at 200 mg/kg of body weight by gavage once daily for 5 days (treatment group). The remaining three mice each received distilled water by gavage once daily for 5 days (control group). Two mice in the treatment group died suddenly during handling approximately 24 h following the last treatment, shortly before the remaining mice were euthanized for sampling. Gross necropsy findings included enteritis in one mouse and mild icterus in the other. Euthanasia of the remaining mice was accomplished by isoflurane exposure, and tissues were harvested aseptically from all mice. One-third of each bladder from the treated mice was submitted to the Prairie Diagnostic Services Toxicology Laboratory to quantify gallium concentrations in tissue homogenate by inductively coupled plasma mass spectrometry.

Confirmation of infection. Tissues were stored at −20°C prior to microbiological culture, which was performed within 24 h of sample collection. Samples from kidneys and bladders were plated on MacConkey II agar (BD Canada, Mississauga, ON, Canada) and on Trypticase soy agar with 5% sheep blood (BD Canada) and incubated at 37°C for 18 to 24 h. Identification was based on colony type and morphology, Gram-staining characteristics, and growth on MacConkey II agar.

Synchrotron X-ray fluorescence imaging and X-ray absorption spectroscopy. X-ray fluorescence maps and X-ray absorption spectra were collected using the Pacific Northwest Consortium/X-ray Science Division (PNC/XSD 20 ID) beamline at the Advanced Photon Source located at Argonne National Laboratory (26). Formalin-fixed, paraffin-embedded tissue from each mouse was sectioned at 20 μm and mounted on high-purity quartz slides (SPI Supplies, West Chester PA). Adjacent sections cut at 5 to 7 μm and stained with hematoxylin and eosin were used for light microscopy to confirm map locations. For XRF and XAS, incident energy was selected with a double-crystal Si(111) monochromator, with the second crystal detuned by 10% for harmonic rejection. Gallium metal foil was used for energy calibration prior to and during data collection. Kirkpatrick-Baez mirrors were used to focus the beam to 5 μm by 5 μm. X-ray fluorescence data were collected at 11 keV with a 10-s integration time and 5-μm horizontal and vertical steps. A minimum area of 20,000 μm^2 was mapped for each sample. Gallium, iron, and zinc Kα fluorescence signals were monitored using a 7-element germanium detector (Canberra Industries, Inc., Meriden, CT) positioned at 45° to the sample and at 90° to the incident beam. X-ray absorption spectra at the Ga K-edge were collected from each sample at regions with the strongest Ga signal using 0.5-eV steps and an integration time of 5 s. At least two spectra were collected at each region.

Data reduction and statistical analysis. Gallium and iron XRF data were processed using ImageJ software (27). Due to the proximity of the gallium Kα and zinc Kα emission energy ranges, the gallium data were corrected for the influence of the zinc signal prior to correlation analysis. Counts for gallium Kα emission were collected between 9.04 keV and 9.28 keV, and counts for zinc Kα emission were collected between 8.36 keV and 8.92 keV. The detector resolution was approximately 200 eV over the range of these emission ranges. Assuming that the emission energy had a Gaussian distribution about the tabulated energy for the emission line, counts from the zinc signal falling in the gallium Kα count window were estimated and then subtracted from the counts recorded in the gallium Kα window. The iron signals and zinc-corrected gallium signals were normalized to the incident beam intensity (I_0) prior to plotting element distribution maps. Spearman's correlation was used to evaluate the relationship between I_0-normalized corrected counts in the gallium Kα emission range and the I_0-normalized counts in the iron Kα emission range at each pixel from XRF maps. This analysis was conducted with a commercial statistical software package (Stata/IC 10.1 for Windows; StataCorp, College Station TX).

Near-edge spectra collected at the gallium K-edge from the regions of strongest gallium fluorescence signal were processed using OriginPro 8.5 (OriginLab Corporation, Northampton, MA) and the XAS data-processing software Athena (28). Spectra were normalized to I_0, and energy values were calibrated using data collected simultaneously from gallium foil. After spectra were averaged, a pre-edge background was subtracted and a polynomial was fitted to the postedge region. The Athena flattening algorithm was then applied to reduce the slope in the postedge line.

TABLE 1 Gallium concentrations in homogenized bladder and Spearman's rho for gallium and iron counts in XRF maps obtained from mice with urinary tract infections following gallium maltolate administration by gavage at 200 mg/kg/day for 5 days

Mouse	Gallium concn (μg/g)	Spearman's rho (*P* value)
A	1.90	0.60 (<0.0001)
B	2.30	0.86 (<0.0001)
C	1.93	0.74 (<0.0001)

RESULTS

Microbiology. Bacterial growth consistent with *E. coli* was observed from the bladders of all control mice. No bacterial growth was observed from the bladders from mice treated with gallium maltolate. There was no bacterial growth from the kidneys of any mice, indicating that the infection model was limited to cystitis.

Localization of gallium in bladder. The median gallium concentration in homogenized tissue samples was 1.93 μg/g (Table 1). X-ray fluorescence at the gallium K-edge was detected in tissue samples from all treated mice. X-ray absorption spectra were collected at the gallium K-edge from the regions with the strongest gallium Kα signal from each mouse (Fig. 1). The sharp increase in X-ray fluorescence around 10.37 keV is characteristic for gallium and confirmed the presence of this element in the mapped regions from the treated mice. The inflection point identified on the first derivative plot of the spectra was located at 10.374 keV for all treated mice. The XRF maps revealed a nonhomogeneous distribution of gallium within the mucosa (Fig. 2a and b). Regions of strong fluorescence in the Ga Kα window were not observed in tissues from the control mice. In treated mice, the gallium distribution was similar but not identical to the iron distribution (Table 1 and Fig. 2c and d).

DISCUSSION

These results are consistent with previous studies which demonstrated absorption of gallium after oral administration of gallium maltolate (19, 29). The mean gallium concentration in homogenized bladder samples from treated mice was approximately five times the serum concentrations reported after oral administration

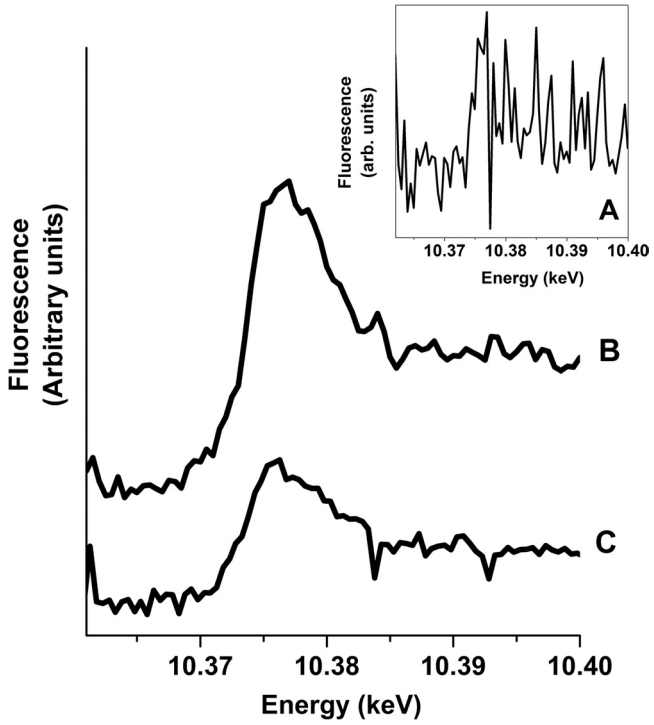

FIG 1 X-ray absorption spectra from regions of strong gallium fluorescence in bladder tissue from three mice treated with gallium maltolate. Letters beside the spectra indicate individual mice. The inset for mouse A uses an expanded *y*-axis scale to facilitate observation of the small edge jump at the gallium K-edge in this sample.

of 50 mg/kg (one-quarter of the dose used in the present study) (29). The mean tissue concentration in this study exceeds the concentrations required to inhibit growth of *Pseudomonas aeruginosa* and *Mycobacterium tuberculosis in vitro*, suggesting that oral administration of gallium maltolate can produce potentially clinically relevant gallium concentrations in homogenized bladder tissue (17, 18). Further characterization of the antimicrobial activity of gallium maltolate against UPEC, including determination of MICs, will be important to better predict its potential clinical utility for treating urinary tract infections caused by UPEC.

Gallium concentrations in homogenized tissue samples are useful to rule out gallium compounds as potential therapeutic agents, since if no gallium is detectable in the sample, it is unlikely that it achieves relevant concentrations in any part of the tissue. As homogenized samples contain all tissue layers, researchers cannot distinguish gallium within the target region of the sample from gallium in other regions of the sample. The hard X-ray microprobe results confirm that gallium reaches the bladder mucosa after gallium maltolate administration and thus meets one of the basic requirements of an antimicrobial compound: it arrives at the site of infection.

Gallium distribution has previously been ascribed in large part to iron transport mechanisms, particularly transferrin-mediated pathways (14). Gallium and iron share numerous chemical characteristics, such as ionic radius and valence states, and these similarities contribute to similarities in their interactions with other atoms and molecules (14). In the present study, the Spearman's rho values of less than 0.9 between iron and gallium signals from treated mice suggest that, in the bladder, gallium is partially distributed via mechanisms that do not involve iron. Observations in bone marrow, liver, spleen, and tumor tissues have similarly indicated that gallium and iron are not identically distributed in tissues (15). The positive values obtained for Spearman's rho suggest that inhibition of one metal's distribution by the other is not a large component of the relationship between gallium and iron in the bladder. This is consistent with a common high-capacity transport system coupled with additional specific pathways to account for the differences in distribution. The common distribution pathway may include transferrin and transferrin receptors, as previously described, while the greater aqueous solubility of gallium than of iron at physiological pH may explain differences in the distribution of non-protein-bound gallium and iron (15).

Iron transport in mammalian tissues is heavily dependent on transferrin and its receptors and on transporters from solute carrier family 11, notably SLC11A2 (divalent metal transporter-1) and SLC11A3 (ferroportin) (30, 31). Iron uptake via transferrin receptors involves endocytosis, release from transferrin, reduction, and subsequent transport of ferrous iron out of the vesicles by SLC11A2 (32). While SLC11A2 will accept a variety of divalent cations as substrates, ferric iron must be reduced to its ferrous form before it can be transported (31). It is unlikely that gallium, present as a trivalent cation unable to be reduced under physiological conditions, would be efficiently transported by SLC11A2 or SLC11A3. Characterization of the transport mechanisms for gallium will be essential for predicting gallium distribution within other tissue types and for identifying potential drug-drug or drug-nutrient interactions that could lead to clinically significant alterations in pharmacokinetics. Additional hard X-ray microprobe studies may provide critical insight into gallium transport mechanisms by revealing intracellular distribution and chemistry.

To our knowledge, this is the first application of synchrotron-based techniques to the identification of antimicrobial distribution within tissues. The simultaneous mapping of multiple elements of interest by synchrotron XRF imaging provides information not only about the distribution of a single element but also about the distributional relationships between elements. This capability is useful at the level of tissues, as was accomplished in this experiment, and improvements in spatial resolution should make synchrotron XRF imaging an even more useful method for tracking elemental distribution within biological samples. In this study, we used a spatial resolution of 5 μm, which is suitable for mapping elements in tissues and allows the analysis of larger regions of the sample in the limited available instrument access time. However, spatial resolutions of less than 100 nm have been reported, with speculation that 30-nm resolution should soon be possible (33). Accompanied by method refinements to ensure correct identification of cellular elements, this spatial resolution should allow the characterization of intracellular elemental distribution without the need to disrupt tissue architecture.

The utility of XAS in hard X-ray microprobe analysis of tissues extends beyond confirming the presence of a specific element. The spectra collected in this study, particularly those from mice B and C, are of sufficient quality to suggest that the determination of gallium species is possible in these samples. The edge energy inflection point, approximately 7 eV above the tabulated electron binding energy for the gallium K-edge, is similar to previously

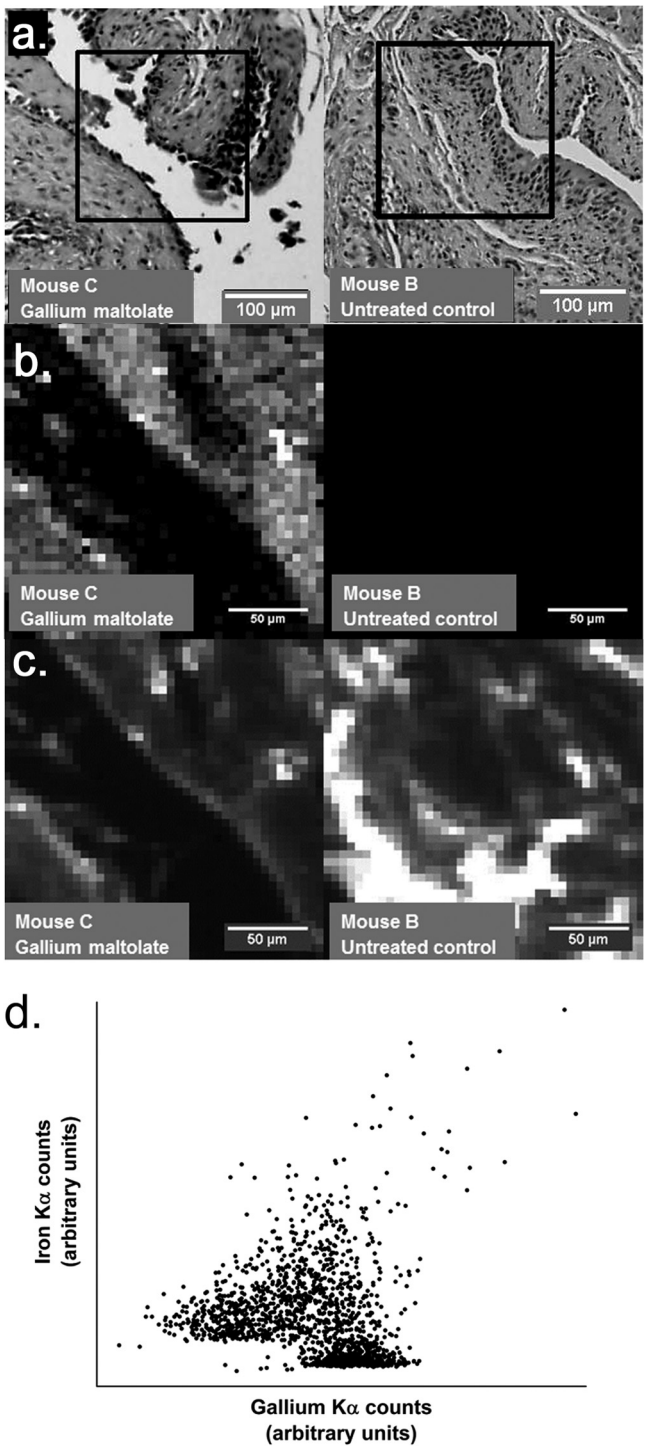

FIG 2 Visible-light microscopy images, gallium distribution maps, and iron distribution maps of selected regions of bladder tissue from a mouse treated with gallium maltolate and an untreated control mouse. (a) Hematoxylin-and-eosin-stained sections of bladder tissue from mouse C treated with gallium maltolate and untreated control mouse B. The regions represented in panels b and c are outlined. (b) Synchrotron X-ray fluorescence maps of gallium distribution in bladder tissue from gallium maltolate-treated mouse C and from untreated control mouse B. These maps were collected from the regions outlined in panel a. The relative fluorescence signal intensity at each pixel is indicated by a color gradient where white represents a strong signal (indicating high local gallium concentration) and black represents a weak signal; both images employ identically calibrated scales. The region of weak signals extending from the upper left corner to the lower right corner in the map from mouse C (left) corresponds to the bladder lumen. (c) Synchrotron X-ray fluorescence maps of iron distribution in bladder tissue from gallium maltolate-treated mouse C and untreated control mouse B. These maps were collected from the same locations shown in panels a and b. The relative fluorescence signal intensity at each pixel is indicated by a color gradient where white represents strong signals (indicating high local iron concentration) and black represents a weak signal; both images employ identically calibrated scales. (d) Scatter plot of iron counts versus gallium counts at each pixel in the X-ray fluorescence maps collected from gallium maltolate-treated mouse C (panels a, b, and c). Spearman's rho for this data set is 0.74 ($P < 0.0001$).

reported observations for Ga_2O_3 and for $Ga(NO_3)_3$ (34, 35). While these spectroscopy results are preliminary, they demonstrate that near-edge X-ray absorption spectroscopy is possible and that extended X-ray absorption fine-structure spectroscopy (EXAFS) may be possible at the gallium K-edge in tissue samples despite the low gallium concentrations observed during treatment. Additional XAS studies of gallium at the site of infection will allow the refinement of *in vitro* antimicrobial susceptibility testing strategies by providing the necessary information to more closely reproduce the chemistry of the site of infection.

Along with the negative bladder cultures from the control mice, positive bladder cultures from all of the control mice suggest that gallium maltolate administration leads to antimicrobial activity in the bladder tissues. While only a small number of mice were included in this experiment, these results are consistent with findings by other research groups that gallium maltolate administration reduces bacterial loads in tissues (29, 36). Along with *in vitro* pharmacodynamic investigations, further study with larger groups of animals is required to more accurately characterize the antimicrobial activity of gallium maltolate in tissues. In addition to this, the unexpected death of two gallium maltolate-treated mice in the present study should prompt toxicological investigations of this compound. While enteritis and icterus are not classical signs of gallium toxicity, we cannot exclude with certainty the potential of toxicity (37). This is particularly true where few toxicology data are available for comparison and where very small groups of animals were involved. Toxicological characterization of gallium maltolate will be essential for determining whether this compound should be considered further as a candidate for clinical use as an antimicrobial therapy.

The distribution characteristics of gallium in the urinary bladder following oral administration of gallium maltolate suggest that this compound may be a suitable candidate for further development as an antimicrobial therapy for UTIs caused by UPEC. This is further supported by its apparent antimicrobial efficacy in a small group of mice, but further efficacy studies using larger groups will be necessary to confirm this observation. Toxicology investigations are indicated to establish whether gallium maltolate may exert unacceptable toxic effects at potentially therapeutic doses. Elucidation of the major uptake and transport mechanisms for gallium will be essential for predicting potential drug-nutrient and drug-drug interactions, as the behavior of iron does not accurately reflect the behavior of gallium. As XRF imaging and *in situ* XAS techniques evolve to provide spatial resolution in the 30-nm range, studies of the intracellular distribution and chemistry of gallium should aid in directing investigations of the mechanisms of gallium transport and uptake.

ACKNOWLEDGMENTS

We thank J. Y. Ko and Robert Gordon for their assistance with data collection at the Advanced Photon Source and Lawrence Bernstein for providing gallium maltolate.

This research was supported by a Collaborative Health Research Projects grant from NSERC and CIHR. K.R.B. and F.S. are CIHR Fellows in Health Research Using Synchrotron Techniques. K.R.B. is supported by an Interprovincial Graduate Student fellowship. The PNC/XSD facilities at the Advanced Photon Source and research at these facilities are supported by the U.S. Department of Energy—Basic Energy Sciences, a Major Resources Support grant from NSERC, the University of Washington, Simon Fraser University, and the Advanced Photon Source. Use of the Advanced Photon Source, an Office of Science User Facility operated for the U.S. Department of Energy (DOE) Office of Science by Argonne National Laboratory, was supported by the U.S. DOE under contract no. DE-AC02-06CH11357.

Experimental work was conducted at the Western College of Veterinary Medicine (University of Saskatchewan, Saskatoon, Saskatchewan, Canada) and at the Advanced Photon Source (Argonne National Laboratory, Argonne, IL, USA).

REFERENCES

1. **Laupland KB, Ross T, Pitout JD, Church DL, Gregson DB.** 2007. Community-onset urinary tract infections: a population-based assessment. Infection **35:**150–153.
2. **Ball KR, Rubin JE, Chirino-Trejo M, Dowling PM.** 2008. Antimicrobial resistance and prevalence of canine uropathogens at the Western College of Veterinary Medicine Veterinary Teaching Hospital, 2002-2007. Can. Vet. J. **49:**985–990.
3. **Foxman B.** 2003. Epidemiology of urinary tract infections: incidence, morbidity, and economic costs. Dis. Mon. **49:**53–70.
4. **Low DA, Braaten BA, Ling GV, Johnson DL, Ruby AL.** 1988. Isolation and comparison of *Escherichia coli* strains from canine and human patients with urinary tract infections. Infect. Immun. **56:**2601–2609.
5. **Kurazono H, Nakano M, Yamamoto S, Ogawa O, Yuri K, Nakata K, Kimura M, Makino S, Nair GB.** 2003. Distribution of the usp gene in uropathogenic *Escherichia coli* isolated from companion animals and correlation with serotypes and size-variations of the pathogenicity island. Microbiol. Immunol. **47:**797–802.
6. **Johnson JR, Clabots C.** 2006. Sharing of virulent *Escherichia coli* clones among household members of a woman with acute cystitis. Clin. Infect. Dis. **43:**e101–e108.
7. **Gupta K, Hooton TM, Wobbe CL, Stamm WE.** 1999. The prevalence of antimicrobial resistance among uropathogens causing acute uncomplicated cystitis in young women. Int. J. Antimicrob. Agents **11:**305–308.
8. **Karlowsky JA, Kelly LJ, Thornsberry C, Jones ME, Sahm DF.** 2002. Trends in antimicrobial resistance among urinary tract infection isolates of *Escherichia coli* from female outpatients in the United States. Antimicrob. Agents Chemother. **46:**2540–2545.
9. **Nys S, Terporten PH, Hoogkamp-Korstanje JA, Stobberingh EE.** 2008. Trends in antimicrobial susceptibility of Escherichia coli isolates from urology services in The Netherlands (1998-2005). J. Antimicrob. Chemother. **62:**126–132.
10. **Wiles TJ, Kulesus RR, Mulvey MA.** 2008. Origins and virulence mechanisms of uropathogenic *Escherichia coli.* Exp. Mol. Pathol. **85:**11–20.
11. **Schilling JD, Lorenz RG, Hultgren SJ.** 2002. Effect of trimethoprim-sulfamethoxazole on recurrent bacteriuria and bacterial persistence in mice infected with uropathogenic *Escherichia coli.* Infect. Immun. **70:**7042–7049.
12. **Blango MG, Mulvey MA.** 2010. Persistence of uropathogenic *Escherichia coli* in the face of multiple antibiotics. Antimicrob. Agents Chemother. **54:**1855–1863.
13. **Emody L, Kerenyi M, Nagy G.** 2003. Virulence factors of uropathogenic *Escherichia coli.* Int. J. Antimicrob. Agents **22**(Suppl 2):29–33.
14. **Bernstein LR.** 1998. Mechanisms of therapeutic activity for gallium. Pharmacol. Rev. **50:**665–682.
15. **Weiner RE.** 1996. The mechanism of 67Ga localization in malignant disease. Nucl. Med. Biol. **23:**745–751.
16. **Emery T.** 1986. Exchange of iron by gallium in siderophores. Biochemistry **25:**4629–4633.
17. **Kaneko Y, Thoendel M, Olakanmi O, Britigan BE, Singh PK.** 2007. The transition metal gallium disrupts *Pseudomonas aeruginosa* iron metabolism and has antimicrobial and antibiofilm activity. J. Clin. Invest. **117:**877–888.
18. **Olakanmi O, Britigan BE, Schlesinger LS.** 2000. Gallium disrupts iron metabolism of mycobacteria residing within human macrophages. Infect. Immun. **68:**5619–5627.
19. **Bernstein LR, Tanner T, Godfrey C, Noll B.** 2000. Chemistry and pharmacokinetics of gallium maltolate, a compound with high oral gallium bioavailability. Met. Based Drugs **7:**33–47.
20. **Berry JP, Poupon MF, Galle S, Escaig F.** 1984. Role of lysosomes in gallium concentration by mammalian tissues. Biol. Cell **51:**43–51.
21. **Palmer BM, Vogt S, Chen Z, Lachapelle RR, Lewinter MM.** 2006. Intracellular distributions of essential elements in cardiomyocytes. J. Struct. Biol. **155:**12–21.
22. **Rao DV, Swapna M, Cesareo R, Brunetti A, Akatsuka T, Yuasa T, Takeda T, Tromba G, Gigante GE.** 2009. Investigation of the distribution of elements in snail shell with the use of synchrotron-based, micro-beam X-ray fluorescence spectrometry. J. Trace Elem. Med. Biol. **23:**251–257.
23. **Ishihara R, Ide-Ektessabi A, Ikeda K, Mizuno Y, Fujisawa S, Takeuchi T, Ohta T.** 2002. Investigation of cellular metallic elements in single neurons of human brain tissues. Neuroreport **13:**1817–1820.
24. **Wagner D, Maser J, Moric I, Boechat N, Vogt S, Gicquel B, Lai B, Reyrat JM, Bermudez L.** 2005. Changes of the phagosomal elemental concentrations by *Mycobacterium tuberculosis* Mramp. Microbiology **151:**323–332.
25. **Mulvey MA, Lopez-Boado YS, Wilson CL, Roth R, Parks WC, Heuser J, Hultgren SJ.** 1998. Induction and evasion of host defenses by type 1-piliated uropathogenic *Escherichia coli.* Science **282:**1494–1497.
26. **Heald S, Cross J, Brewe D, Gordon R.** 2007. The PNC/XOR X-ray microprobe station at APS sector 20. Nucl. Instrum. Methods Phys. Res. A **582:**215–217.
27. **Abràmoff MD, Magalhães PJ, Ram SJ.** 2004. Image processing with imageJ. Biophotonics Int. **11:**36–41.
28. **Ravel B, Newville M.** 2005. ATHENA, ARTEMIS, HEPHAESTUS: data analysis for X-ray absorption spectroscopy using IFEFFIT. J. Synchrotron Radiat. **12:**537–541.
29. **Harrington JR, Martens RJ, Cohen ND, Bernstein LR.** 2006. Antimicrobial activity of gallium against virulent *Rhodococcus equi* in vitro and in vivo. J. Vet. Pharmacol. Ther. **29:**121–127.
30. **Gunshin H, Fujiwara Y, Custodio AO, Direnzo C, Robine S, Andrews NC.** 2005. Slc11a2 is required for intestinal iron absorption and erythropoiesis but dispensable in placenta and liver. J. Clin. Invest. **115:**1258–1266.
31. **Wang J, Pantopoulos K.** 2011. Regulation of cellular iron metabolism. Biochem. J. **434:**365–381.
32. **MacKenzie EL, Iwasaki K, Tsuji Y.** 2008. Intracellular iron transport and storage: from molecular mechanisms to health implications. Antioxid. Redox Signal. **10:**997–1030.
33. **Matsuyama S, Shimura M, Mirnura H, Fujii M, Yumoto H, Sano Y, Yabashi M, Nishino Y, Tamasaku K, Ishikawa T, Yamauchi K.** 2009. Trace element mapping of a single cell using a hard x-ray nanobeam focused by a Kirkpatrick-Baez mirror system. X Ray Spectrom. **38:**89–94.
34. **Meitzner GD, Iglesia E, Baumgartner JE, Huang ES.** 1993. The chemical-state of gallium in working alkane dehydrocyclodimerization catalysts—in situ gallium K-edge X-ray absorption-spectroscopy. J. Catal. **140:**209–225.
35. **Faro AC, Eon JG, Nogueira L, da Silva RF, Rodrigues VD.** 2008. XAFS study of H-ZSM5 catalysts modified with gallium. Catal. Today **133:**913–918.
36. **DeLeon K, Balldin F, Watters C, Hamood A, Griswold J, Sreedharan S, Rumbaugh KP.** 2009. Gallium maltolate treatment eradicates *Pseudomonas aeruginosa* infection in thermally injured mice. Antimicrob. Agents Chemother. **53:**1331–1337.
37. **Collery P, Keppler B, Madoulet C, Desoize B.** 2002. Gallium in cancer treatment. Crit. Rev. Oncol. Hematol. **42:**283–296.